ENTOMOLOGICAL Communications

Entomological Communications, 7, 2025: ec07033
doi: 10.37486/2675-1305.ec07033
e-ISSN: 2675-1305
Open Access Full Text Article

Protocol & Techniques

A Low-Cost Shape-from-Focus Workflow for 3D Geometric Morphometrics: Proof of Concept Using *Trypoxylus dichotomus* (Linnaeus, 1771) (Coleoptera: Scarabaeidae) Genitalia

Wonseok Choi

The Diversity of Small Worlds, Seoul, Republic of Korea.
Corresponding author: won0507won@gmail.com

Edited by: Jorge L. P. Souza

Received: September 10, 2025. Accepted: November 24, 2025. Published: December 10, 2025.

Abstract. Two-dimensional (2D) photography is widely used in geometric morphometrics (GM), but loss of information and orientation errors remain concerns in volumetric structures. Three-dimensional (3D) imaging provides more accurate shape representations for such structures, but it typically requires expensive equipment. We developed a low-cost automated workflow based on a shape-from-focus (SFF) algorithm to reconstruct partial 3D surfaces from uniformly stepped focus stacks. As a proof of concept, we applied this method to the male genitalia of *Trypoxylus dichotomus* (Linnaeus, 1771) (Coleoptera: Scarabaeidae), comparing 2D and 3D landmark analyses. The reconstructed 3D models yielded reliable regions for landmark and semilandmark placement. Both 2D and 3D analyses revealed consistent hypoallometric scaling, but the choice of size proxy (3D centroid size versus linear length) had a greater impact on allometric inference than the dimensionality of landmarks. The SFF workflow provides a rapid and inexpensive alternative for generating 3D models suitable for GM, and highlights the importance of validating 2D measures against centroid-based proxies.

Keywords: landmark dimensionality, size proxy, morphology, allometry.

Geometric morphometrics (GM) has become an essential tool for analyzing shape and its relationships to other biological features, from allometry to phylogeny (Zelditch et al. 2012). GM extracts pure shapes by removing size and rotation information (Kendall 1977; Zelditch et al. 2012). The Procrustes analysis on landmarks is commonly employed based on two-dimensional (2D) photographs to acquire a pure shape (Klingenberg 2016). 2D landmarks are the most widely adopted and are often considered a reasonable proxy for three-dimensional (3D) structures due to various factors, for example, low cost, computational simplicity, and effective visualization (Cardini 2014). Despite the simplicity and extensive application of 2D images, there have been concerns about loss of information due to distortions introduced by photography and by flattening 3D into 2D (Buser et al. 2018; Cardini 2014; Wasiljew et al. 2020).

Recent advancements in 3D scanning technology reduced its costs and increased accessibility. However, micro-computed tomography (CT), which is the gold-standard for 3D scanning, is still expensive and requires more time compared to traditional 2D methods (Wasiljew et al. 2020). Another widely used approach, 3D photogrammetry, reconstructs structures from multi-view images. Although it offers a rapid and cost-effective alternative, its initial set-up requires a considerable investment (Medina et al. 2020). High-resolution 3D surface scanners can achieve micrometer-scale accuracy, but their precision systems are often costly and confined to stationary machinery (Bartol et al. 2021).

The shape from focus (SFF) is used for the estimation of depth using different focus levels of a sequence of images (Noguchi & Nayar 1994). Minute morphology of genital structures can be caught by a sufficiently narrow depth-of-field or by decreasing the distance intervals between each consecutive image. In this paper, an automated algorithm to reconstruct 3D models of mesoscopic structures is proposed, and geometric morphometrics using these models is demonstrated.

Sum Modified Laplacian (SML) focus measurement. To reconstruct 3D models using SFF, a sequence of aligned grayscale and color images was loaded into the workflow for processing. Depth of field (DOF) estimation was performed using the SML focus measure, which exhibits a good performance in various image conditions (Pertuz et al. 2013). For each pixel, the SML values were calculated across the image stack, and the pixels with SML values exceeding the predefined threshold were selected (Fig. 1A-B). Based on the SML information, a color reference image was simultaneously generated by extracting pixel values from the corresponding slice at each selected pixel. The pixel coordinates and associated depth values were passed to the next stage for region construction.

Creation of contours. OpenCV (Bradski 2000) and NumPy (Harris et al. 2020) was used to process images and morphologies. To suppress noise and connect neighboring regions, morphological transformations (dilation followed by erosion) were applied to the pixels with the highest SML values using OpenCV functions. This process merged adjacent selected pixels into continuous focused regions and removes isolated noise (Fig. 1C). To avoid redundancy, overlapping focus regions were removed by comparing each region with its corresponding region in the preceding image slice. Finally, contours of each focus region were extracted for subsequent z-axis estimation using OpenCV function, Canny edge-detection.

To determine the continuity of contours between successive images, Euclidean distances were calculated between a point and its nearest one in the preceding or next images. If the distance is smaller than the predefined threshold, the point and the contour are considered connected to the neighboring image slice.

Placement of reference lines. Points on each contour that were closer to points of adjacent contours than a predefined threshold were regarded as reference points. The line connecting these reference points was defined as the reference line, representing the highest or lowest part of each contour. Contours without close neighbors in the preceding image slice were regarded as the uppermost peaks, whereas those without close neighbors in the subsequent slice were considered the lowest edges of the structure. Contours lacking neighbors in both

the preceding and subsequent slices were assumed to represent small protruding features with heights equal to the focus-step interval of the image stack.

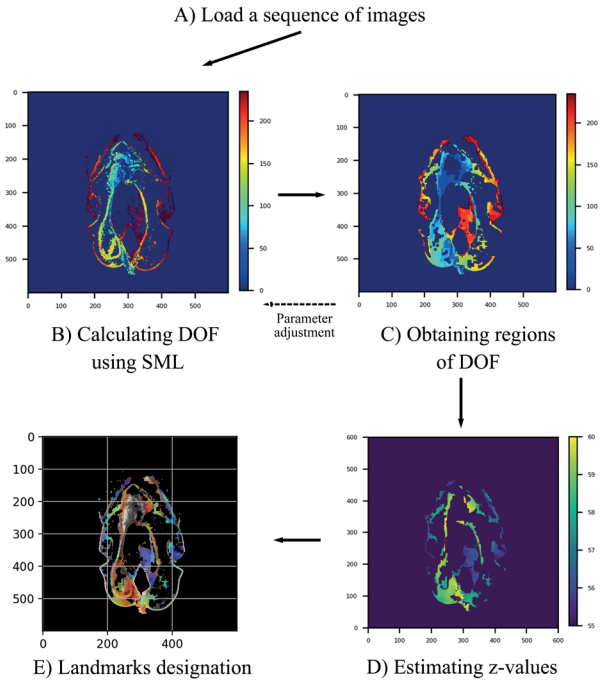

Figure 1. Flow of 3D reconstruction using the shape-from-focus pipeline.

For the uppermost contours, reference lines are generated by iteratively thinning each contour to obtain its morphological skeleton, using OpenCV functions. The morphological skeleton was regarded as the line representing the highest points of the structure. Within the contours corresponding to the lowest edges, all points except those belonging to the reference lines that represent the highest parts were considered the lowest points. All reference lines were visualized using interactive Matplotlib (ver. 3.10.7; Hunter 2007) plots, and an individual reference point can be added or removed manually.

Depth estimation. Points in focus regions are subjected to z-axis estimation. The DOF of an image contains the step length of the height difference. Therefore, using ratios of distances that are between the target point and reference lines, a z-value of the point can be calculated. The distances between a point on the reference line and points on a corresponding reference line are compared. A pair of points with the shortest Euclidean distance is stored as an 'interaction pair.' The target point is projected on the line of the closest interaction pair, and the ratio is calculated based on the projected point.

Geometric morphometrics analysis. Estimated z-values were stored in a depth map, which represents the heights of each pixel (Fig. 1D). Using interactive matplotlib plot functions, landmarks were manually designated on the figure (Figs. 1E and 2). Landmarks were saved in the txt format. The elytron length or centroid size was used as the size proxy to confirm the effect of the dimension of the size proxy. Both 2D and 3D Geometric morphometrics on the parameres and the phallobase were analyzed using R software (R Core Team 2020) with the package geomorph (Adams et al. 2016).

Proof of concept using *Trypoxylus dichotomus* (Linnaeus, 1771) (Coleoptera: Scarabaeidae). As a proof of concept for SFF-based 3D model reconstruction, the male genitalia and elytra of *Trypoxylus dichotomus* were sequentially photographed (n = 15). The median recovery rate, a proportion of pixels within the specimen mask that received valid z-values, from the depth map to the completion of z-values assignment, was 37.0% (IQR 3.55). The algorithm was able to estimate z-values of 7,808 pixels per second on average.

Comparison of landmark- and size-proxy dimensionality. The result revealed statistically significant size hypoallometry in both 2-dimensional (2D) and 3D landmarks against the elytron centroid size (Phallobase, 3D landmarks: β = 0.611 (95% CI 0.398-0.879), $p < 0.0001$, n = 13, Fig. 3A; 2D landmarks: β = 0.639 (95% CI 0.411-0.91), $p < 0.0001$, n = 15; Parameres, 3D landmarks: β = 0.465 (95% CI 0.191-0.784), p = 0.004, n = 15, Fig. 3B; 2D landmarks: β = 0.324 (95% CI 0.153-0.492), p = 0.002, n = 15; Tab. 1). Shapes of the parameres displayed no significant association with the elytron centroid size, however, shapes of the phallobase displayed size-related shape variation, as summarized in Tab. 1 (3D landmarks: R^2 = 0.242 (95% CI 0.098-0.432), p = 0.023; 2D landmarks: R^2 = 0.301 (95% CI 0.113-0.539), p = 0.041).

The choice of size proxy substantially altered the result. An elytron length and a genitalia size showed similar results to those analyzed using the elytron centroid size (Tab. 1). However, using the elytron length as a size proxy resulted in less statistical significance in the phallobase shapes and more significance in the parameres shapes (Fig. 3C-D; 3D phallobase shapes with the elytron length: R^2 = 0.191, p = 0.175; 3D parameres shape with the elytron length: R^2 = 0.159, p = 0.049; Tab. 1). A similar trend was observed in 2D landmarks-based analysis (2D phallobase shapes with the elytron length: R^2 = 0.173, p = 0.192; 2D parameres shape with the elytron length: R^2 = 0.193, p = 0.051; Tab. 1).

The implemented shape-from-focus (SFF) pipeline was designed to reconstruct 3D models from image sequences using inexpensive devices compared to gold-standard 3D imaging systems. Moreover, images can be processed to generate 3D models within minutes. Although low-texture interiors are under-recovered, edges—where

Table 1. Comparison of 3D and 2D landmarks representing shapes and size proxies in geometric morphometrics.

Genital part	Shape dimension	Size proxy (Elytra)	Analysis	Estimation	95% CI		Mean	p-value	
Phallobase	3D	3D centroid size	shape ~ size	R^2	0.098	0.432	0.242	0.023	*
		2D length			0.067	0.384	0.191	0.175	
Parameres		3D centroid size			0.056	0.252	0.126	0.424	
		2D length			0.077	0.285	0.159	0.049	*
Phallobase	2D	3D centroid size			0.113	0.539	0.301	0.041	*
		2D length			0.060	0.359	0.173	0.192	
Parameres		3D centroid size			0.078	0.348	0.183	0.097	
		2D length			0.086	0.333	0.193	0.051	
Phallobase	3D	3D centroid size	size ~ size	slope	0.398	0.879	0.611	<0.0001	***
		2D length			0.470	0.767	0.605	<0.0001	***
Parameres		3D centroid size			0.191	0.784	0.465	0.004	**
		2D length			0.227	0.758	0.465	0.003	**
Phallobase	2D	3D centroid size			0.411	0.910	0.639	<0.0001	***
		2D length			0.525	0.819	0.647	<0.0001	***
Parameres		3D centroid size			0.153	0.492	0.324	0.002	**
		2D length			0.207	0.486	0.345	<0.0001	***

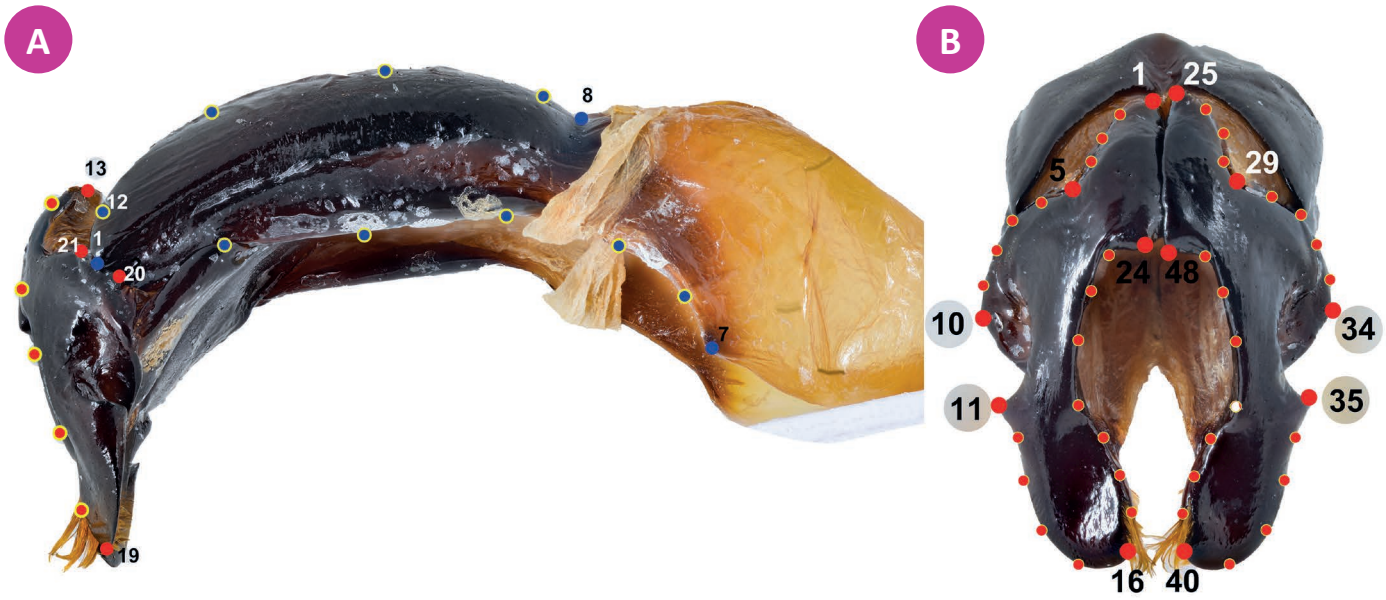

Figure 2. Scheme of landmarks designation on an aedeagus image. A. Lateral view of aedeagus, the landmarks scheme for phallobase. B. Frontal view, the landmarks scheme for parameres.

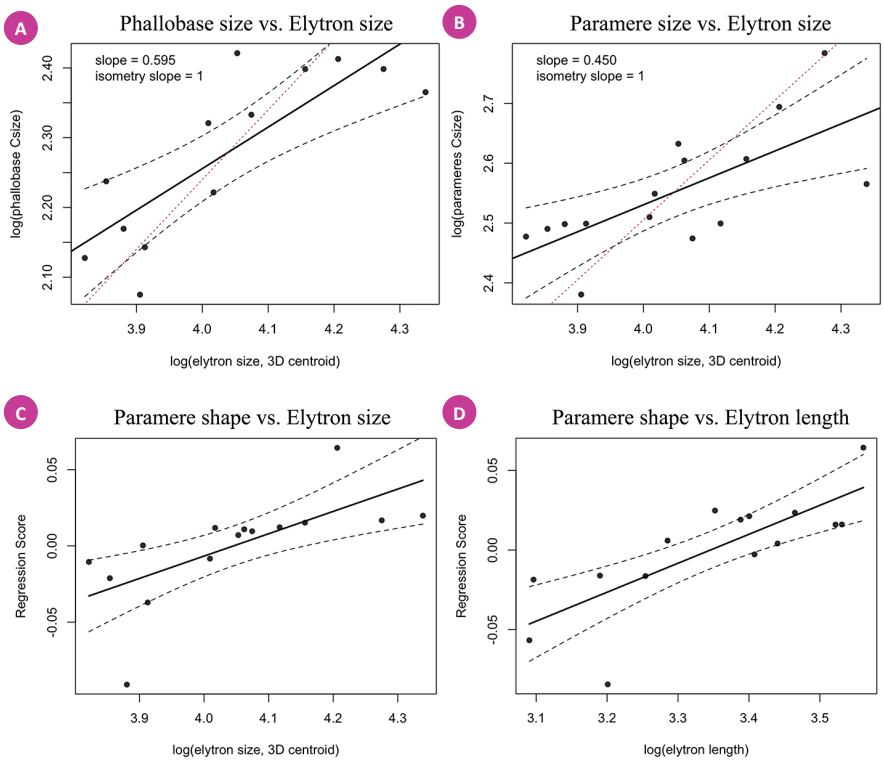

Figure 3. Regression plots of shape models to describe allometry of aedeagus size and shapes. Black dashed lines indicate 95% confidence intervals. A-B. Size allometry of aedeagus sizes and elytron 3D centroid sizes. Red dashed lines indicate the isometry slope. A. Regression plot of phallobase size and elytron size. B. Regression plot of paramere size and elytron size. C-D. Paramere shape and different proxies. C. Regression plot of paramere shape and elytron 3D centroid size. D. Regression plot of paramere shape and elytron length.

most landmarks lie—are reconstructed reliably. Moreover, as the program uses step length and pixel ratios as scales, it is specialized for designating landmarks compared to previous methods that cannot provide the scale (e.g., Falkingham 2012).

These design choices make the approach fast and affordable, but they also limit absolute accuracy relative to gold-standard modalities. Because external benchmarking against high-precision devices was not feasible in this study, we relied on internal quality control and biological performance. The pipeline reproduces consistent genital size allometry in both 2D and 3D landmarks and reveals proxy-sensitive shape allometry. Further study, including external validation, is required to quantify absolute error.

Analyses based on 3D vs 2D shapes yielded concordant conclusions about size allometry, implying that our reconstructed 3D surfaces were as effective as conventional 2D imaging for this purpose. By contrast, the choice of size proxy significantly altered results. The elytral 3D centroid size captures a volumetric aspect of body size, whereas 2D length indexes a single axis. This difference was sufficient to turn effects from significant to non-significant, and *vice versa*. These results emphasize that proxy selection can dominate inference, sometimes more than shape dimensionality itself. Because biological structures are generally three-dimensional, 2D size measures used for shape-size analyses, especially allometry, should ideally be validated against centroid-based proxies when feasible.

Acknowledgments

The author appreciates the National Science Museum, whose *Trypoxylus dichotomus* specimens in the collection were used in the study.

Funding information

No funding received.

Conflict of Interest Statement

The author declares that there are no conflicts of interest.

Data Availability

The code used for the Shape-from-Focus (SFF) 3D reconstruction workflow is available at Zenodo (DOI: https://doi.org/10.5281/zenodo.17486036). It includes all scripts required to reproduce the depth estimation and figure generation described in this study.

References

Adams, D. C.; Collyer, M.; Kaliontzopoulou, A.; Sherratt, E. (2016) Geomorph: Software for geometric morphometric analyses. https://hdl.handle.net/1959.11/21330

Bartol, K.; Bojanić, D.; Petković, T.; Pribanić, T. (2021) A review of body measurement using 3D scanning. *IEEE Access*, 9: 67281-67301. doi: 10.1109/ACCESS.2021.3076595

Bradski, G. (2000). The OpenCV library. *Dr. Dobb's Journal of Software Tools.*

Buser, T. J., Sidlauskas, B. L.; Summers, A. P. (2018) 2D or Not 2D? Testing the Utility of 2D Vs. 3D Landmark Data in Geometric Morphometrics of the Sculpin Subfamily Oligocottinae (Pisces; Cottoidea). *The Anatomical Record*, 301(5): 806-818. doi: 10.1002/ar.23752

Cardini, A. (2014) Missing the third dimension in geometric morphometrics: how to assess if 2D images really are a good proxy for 3D structures? *Hystrix the Italian Journal of Mammalogy*, 25(2): 9. doi: 10.4404/hystrix-25.2-10993

Falkingham, P. L. (2012) Acquisition of high resolution three-dimensional models using free, open-source, photogrammetric software. *Palaeontologia Electronica*, 15: 15.1.1T. doi: 10.26879/264

Harris, C. R.; Millman, K. J.; van der Walt, S. J.; Gommers, R.; Virtanen, P.; Cournapeau, D.; Wieser, E.; Taylor, J.; Berg, S.; Smith, N. J., et al. (2020) Array programming with NumPy. *Nature*, 585(7825): 357-362. doi: 10.1038/s41586-020-2649-2

Hunter, J. D. (2007) Matplotlib: A 2D Graphics Environment. *Computing in Science & Engineering*, 9(3): 90-95. doi: 10.1109/mcse.2007.55

Kendall, D. G. (1977) The diffusion of shape. *Advances in Applied Probability*, 9(3):, 428-430. doi: 10.2307/1426091

Klingenberg, C. P. (2016) Size, shape, and form: concepts of allometry in geometric morphometrics. *Development Genes and Evolution*, 226(3): 113-137. 10.1007/s00427-016-0539-2

Medina, J. J.; Maley, J. M.; Sannapareddy, S.; Medina, N. N.; Gilman, C. M.; McCormack, J. E. (2020) A rapid and cost-effective pipeline for digitization of museum specimens with 3D photogrammetry. *PLOS One*, 15(8): e0236417. doi: 10.1371/journal.pone.0236417

Noguchi, M.; Nayar, S. K. (1994) Microscopic shape from focus using active illumination. In *Proceedings of 12th International Conference on Pattern Recognition,* 1: 147-152. doi: 10.1109/ICPR.1994.576247

Pertuz, S.; Puig, D.; Garcia, M. A. (2013) Analysis of focus measure operators for shape-from-focus. *Pattern Recognition*, 46(5): 1415-1432. doi: 10.1016/j.patcog.2012.11.011

R Core Team (2022) R: A language and environment for statistical computing. R Foundation for Statistical Computing, Vienna, Austria. https://www.r-project.org/

Wasiljew, B. D.; Pfaender, J.; Wipfler, B.; Utama, I. V.; Herder, F. (2020) Do we need the third dimension? Quantifying the effect of the z-axis in 3D geometric morphometrics based on sailfin silversides (Telmatherinidae). *Journal of Fish Biology*, 97(2): 537-545. doi: 10.1111/jfb.14410

Zelditch, M. L.; Swiderski, D. L.; Sheets, H. D. (2012) *Geometric morphometrics for biologists: A primer.* Elsevier Academic Press.